Cellulose Nanofibers for the Enhancement of Printability of Low Viscosity Gelatin Derivatives

Sungchul Shin,[a] Soohyun Park,[a] Minsung Park,[a,c] Eunsue Jeong,[a] Kyunga Na,[a,c] Hye Jung Youn,[b,c] and Jinho Hyun [a,c,d,*]

Inadequate rheological properties of gelatin methacrylamide (GelMA) were successfully improved by incorporating cellulose nanofibers (CNFs), such that the printed scaffolds could maintain their structural fidelity during the three-dimensional (3D) bio-printing process. The CNFs provided an outstanding shear thinning property, and the GelMA/CNF inks exhibited high zero shear viscosity and structural fidelity under a low dispensing pressure. After evaluating the printability, composite inks containing 2% w/v CNF were observed to have an optimal concentration of CNF to prepare 3D print stable constructs. Therefore, these inks were used to manufacture human nose and ear structures, producing highly porous structures in the printed composite hydrogels. Furthermore, the mechanical stability of the GelMA/CNF composite hydrogel was increased when CNFs were incorporated, which indicated that CNFs played an important role in enhancing the structural properties of the composite hydrogels. Additionally, the biocompatibility of CNF-reinforced hydrogels was evaluated using a fibroblast cell line.

Contact information: a: Department of Biosystems and Biomaterials Science and Engineering, Seoul National University, Seoul 151-921, Republic of Korea; b: Department of Forest Science, Seoul National University, Seoul 151-921, Republic of Korea; c: Research Institute of Agriculture and Life Sciences, Seoul National University; d: Center for Food and Bioconvergence, Seoul National University;
* Corresponding author: jhyun@snu.ac.kr

INTRODUCTION

The increasing interest in tissue engineering has heightened the need for a new platform to manufacture 3D bio-printed scaffolds (Dutta and Dutta 2009). These 3D-shaped structures hold great promise for therapies aimed at tissue regeneration and organ repair and replacement (Hollister 2005; Sengers *et al.* 2007; Mironov *et al.* 2009). Cell-cell or cell-matrix interactions can be improved when the cells are encapsulated in 3D porous scaffolds rather than 2D ones (Abbott 2003; Debnath and Brugge 2005; Loessner *et al.* 2010). Hence, considerable research has been devoted to introduce 3D bio-printing techniques with hydrogel based bio-inks and cell encapsulation strategies to prepare 3D porous scaffolds (Murphy and Atala 2014; Markstedt *et al.* 2015). To this end, several criteria must be fulfilled: the bio-inks must have sufficient rheological properties to maintain their structure after printing; printed bio-inks should show proper mechanical properties according to their respective applications; and the bio-inks need to be biocompatible and exhibit low cytotoxicity. By meeting these requirements, personalized tissue engineering can be realized *via* 3D bio-printing techniques.

Gelatin, the partially denatured derivative of collagen, is a promising material for bio-inks, as it resembles the chemical structure and biological functions of collagen in the

native extracellular matrix (ECM). Because of these merits, gelatin has been broadly evaluated for 3D bio-printing applications (Bertassoni *et al.* 2014; Billiet *et al.* 2014). Modified gelatin with pendant methacrylamide groups (GelMA) has been widely investigated because of the ease of radical polymerization and its stable inner network structure after chemical crosslinking. Additionally, GelMA retains natural cell binding motifs, such as RGD peptides, which improve cell-responsive features such as cell adhesion, proliferation, migration, and differentiation (Ruoslahti 1996; Yeo *et al.* 2007; Nichol *et al.* 2010). Some studies have tried to 3D print high concentration GelMA (~20% w/v) under precisely controlled temperature (Billiet *et al.* 2014). However, the most essential features of a scaffold, high porosity with an interconnected pore network to ensure cell growth and the transportation of nutrients, cannot be achieved in high concentration hydrogels (Bertassoni *et al.* 2014). While low concentration GelMA (< 5% w/v) bio-inks ensures a high porosity, they show low zero shear viscosity, which results in the lack of shape and flow stability during the printing process (Colosi *et al.* 2016). Hence, the low viscosity of highly porous GelMA hydrogel appears to be a critical limitation to printing desirable 3D scaffolds.

Cellulose nanofibers (CNF) are nanoscale cellulose fibrils whose typical widths are several tens of nanometers with a wide range of lengths, and their high aspect ratio imparts excellent physical and mechanical properties (Stelte and Sanadi 2009). They can be produced in various ways, such as homogenizing, microfluidizing, grinding, and chemical treatments (Abe *et al.* 2007; Henriksson *et al.* 2008; Park *et al.* 2015). Mechanical fibrillation using a grinder has been widely used due to its distinct advantages compared with chemical treatments. Chemical treatments such as sulfuric acid hydrolysis and TEMPO-mediated oxidation can damage the chain length of cellulose fibers (Saito *et al.* 2007; Shinoda *et al.* 2012). However, CNFs with high aspect ratio can be produced by mechanical grinding without any significant loss of chain length (Abe *et al.* 2007). Highly viscous CNF dispersions with low concentrations of cellulose can be easily produced in a mechanical grinder. Due to their high mechanical strength, CNFs have been widely studied for enhancing the mechanical properties and structural stability of weak hydrogels (Ovsianikov *et al.* 2011; Yang *et al.* 2013).

In this study, CNFs prepared using a mechanical grinder were used to increase the zero shear viscosity of low concentration GelMA precursor solutions. Incorporating CNFs with GelMA acted as not only a viscosity modifier but also a mechanical property enhancer. The shape fidelity of GelMA constructs was effectively improved. The viability of encapsulated fibroblast cells in GelMA/CNF 3D-printed hydrogel was investigated for potential biomedical applications in the future.

EXPERIMENTAL

Materials

The CNF suspensions were produced from craft pulp (Moorim P&P, Ulsan, Korea). Gelatin (Type A from porcine skin, bloom number: 300) was purchased from Sigma-Aldrich Korea (Seoul, Korea).

Methods

Synthesis of gelatin methacrylamide

The GelMA was synthesized by allowing Type A porcine skin gelatin at 10%

(w/v) to dissolve in 50 mL of Dulbecco's phosphate buffered saline (DPBS) (Gibco, Waltham, USA). Next, 3 mL of methacrylic anhydride (Sigma-Aldrich) was added dropwise and reacted at 50 °C for 2 h. The resulting mixture was dialyzed in a cellulose membrane (MWCO 12 to 14 kDa) for 3 days against 50 °C of distilled water (DI water) with frequent water replacement. The dialyzed solution was lyophilized, resulting in a sponge-shaped structure.

Production of cellulose nanofiber (CNF)

Prior to grinding, the pulp fibers were beaten using a laboratory Valley beater for 30 min. The beaten pulp suspension was passed through a grinder (Super Masscolloider, Masuko Sangyo Co., Ltd, Kawaguchi, Japan) to produce the CNF suspension. The consistency of the pulp suspension during grinding was 2% w/v. The operational speed and gap distance between the grinder stones were 1500 rpm and -100 µm, respectively. The number of passes through the grinder was fixed at 30.

GelMA/CNF bio-ink preparation

To prepare the bio-ink precursor solution, the concentrated CNFs were mixed intensely and steam sterilized (100 kPa at 120 °C for 20 min) in an autoclave. Five different concentrations of CNF solution (0, 0.5, 1.0, 1.5, and 2.0% w/v) were prepared in 3T3 cell culture medium (Dulbecco's minimal essential medium (DMEM) with 4.5 g/L glucose, L-glutamine, sodium pyruvate, and 10% fetal bovine serum (FBS)) with 5% w/v GelMA dissolved in the solutions. Ammonium persulfate (APS) (Sigma-Aldrich), used as a radical initiator, was purified through distillation under reduced pressure and recrystallization and then added to the CNF solutions at different concentrations (0, 2.5, 5, 7.5, 10, 15, 20, and 40 mM) to crosslink the GelMA after 3D printing. Activation of radicals was performed by adding the same concentration of tetramethylethylenediamine (TEMED) (Sigma-Aldrich) as APS.

Characterization of chemical structures of GelMA/CNF

The chemical structures of the samples were characterized by Fourier transform infrared spectroscopy (FT-IR spectroscopy, Nicolet iS5, Thermo Scientific, Waltham, MA USA). The scan number was 32, with a resolution of 8 cm^{-1} and the wavenumber range of 4000 to 600 cm^{-1}.

Rheological measurements of bioinks and composite hydrogels

GelMA/CNF composite precursor solutions containing 5% w/v of GelMA and variable concentrations up to 2.0% w/v of CNF were prepared by dissolving the polymers in the cell culture medium. The rheological behavior of the GelMA/CNF hydrogel inks was analyzed using a digital rheometer (MARSIII, Thermo Scientific, Waltham, USA) fitted with parallel plate geometry (35-mm radius) to investigate the possible shear thinning properties. To study the shear viscosity of the bio-inks, 1.0 mL was poured into the geometry at 25 °C, and the measurement was performed in Rot Ramp mode (shear rates 0.01 to 1000 s^{-1} with a gap size 1.0 mm). To identify the linear viscoelastic region, the samples were subjected to stress sweep experiments at 25 °C employing a stress range from 0.1 to 1000 Pa and a frequency of 1 Hz.

Viscoelastic properties of composite hydrogels after chemical crosslinking were measured using the same digital rheometer. GelMA/CNF composite precursor solutions containing 5% w/v of GelMA and variable concentrations up to 2.0% w/v of CNF were

prepared by dissolving the polymers in the 3T3 cell culture medium. A composite bio-ink was injected into a glass mold, which had a gap size of 1.6 mm and allowed complete chemical crosslinking. Circular gel discs (8 mm in diameter) were produced from the gel slabs using a biopsy punch. The oscillatory rheometry in the shear strain-sweep mode was performed with 1 Hz frequency. The gel moduli were measured using parallel plate geometry (8 mm) with a nominal force of 0.2 N and gap size of 1.6 mm.

3D Printing of bioinks

The 3D structures were fabricated by printing patterns using a custom-built 3D printer. The patterns were designed using the commercially available Rhinoceros software (version 5.0, Seattle, USA). The respective codes were translated into G-code instructions for the deposition stage using a custom Visual Basic program. The composite bio-inks, which had various CNF concentrations, were loaded in a 5 mL syringe fitted with a 160-μm inner diameter nozzle. The flow rate was controlled by adjusting the dispensing pressure (1.0 to 10 psi) and the dosing distance (0.05 to 0.1 mm). Four shapes were constructed in a Petri dish: a hollow cube (10×10 mm^2, 40% infill density, 0.4 mm layer height, and a printing speed of 10 mm s^{-1}), a human nose (25.6×38.3 mm^2, 40% infill density, 0.4 mm layer height, printing speed 10 mm s^{-1}, and a printing time of approximately 17 min), a human ear (24.2×26.2 mm^2, 40% infill density, 0.4 mm layer height, printing speed 10 mm s^{-1}, and a printing time of approximately 13 min), and a mesh (20×20 mm^2, 40% infill density, 0.4 mm layer height, and a printing speed of 10 mm s^{-1}). The hollow cubes were 3D printed with five GelMA/CNF inks, which contained 5% w/v of GelMA and different concentrations of CNF (0, 0.5, 1.0, 1.5, and 2.0% w/v) to evaluate their printability. The more complex 3D structures, such as the nose and ears, were 3D printed with 2% w/v of CNF-incorporated GelMA/CNF bioinks.

Determination of gelation time

To control the gelation time, APS and TEMED were added at variable concentrations (0, 2.5, 5, 7.5, 10, 15, 20, and 40 mM) into 5% w/v GelMA and 2% w/v CNF solutions dissolved in PBS buffer at 37 °C. Then 50 μL of mixture solutions were dropped into a 96 well plate. Gelation times of GelMA/CNF bio-inks were determined as a starting point of an abrupt increase in the turbidity curves measured using a UV-vis spectrophotometer (Synergy HT, BioTek, Winooski, USA) with a temperature controller.

Imaging of morphology and microstructure

The morphologies of the freeze-dried GelMA, CNF, and GelMA/CNF hydrogels were analyzed using a field-emission scanning electron microscopy (FE-SEM; SUPRA 55VP, Carl Zeiss, Oberkochen, Germany) at an operation voltage of 2 kV. Platinum was sputtered onto the composite hydrogels at 20 mV for 160 s as a conductive coating for imaging purposes. The 3D printed structures were immersed in the liquid nitrogen immediately after the printing to maintain the porosity.

Mechanical properties of composite hydrogels

The mechanical properties of the composite hydrogels were investigated by compression testing using a universal testing machine (UTM, GB/LRX Plus, Lloyd, West Sussex, UK) fitted with a 10 N load cell. For the compression testing, 8 mm diameter and 160 μm height cylindrical samples were prepared and compressed to 40% of their

original thickness, with a constant crosshead speed of 2 mm/min at room temperature.

Cytotoxicity of composite hydrogels

To study the cellular behavior encapsulated in the composite hydrogels, 1.5×10^6 cells/mL NIH 3T3 cells were added to the composite bio-inks. Cell-laden composite bio-inks containing APS/TEMED were loaded to a 5 mL syringe and 3D printed to form mesh structures. After the gelation of GelMA, the printed structures were cultured in medium. The culture medium consisted of DMEM with 4.5 g/L glucose, L-glutamine, sodium pyruvate, and 10% FBS. The cells encapsulated in the composite hydrogels were cultured in a humidified 5% CO_2 incubator at 37 °C for 1, 4, and 7 days. To investigate the viability of the encapsulated cells, a live and dead viability/cytotoxicity kit (Invitrogen, Waltham, USA) was used. The indicated combined live and dead assay reagents were added to a Petri dish containing cell laden constructs, and the mixture was incubated for 1 h at room temperature in the dark. Green (live cells) and red (dead cells) fluorescence images were collected separately using a fluorescence microscope (BX51, Olympus, Tokyo, Japan). Nonspecific cellular metabolic activity was measured using alamar blue. Cell/hydrogel constructs were washed once with PBS and incubated with alamarBlue® (Invitrogen, Waltham, USA) solution for 4 h at 37 °C. The alamarBlue® fluorescence was assayed at 540 nm (excitation) and 590 nm (emission) using a microplate reader (Synergy HT, BioTek, Winooski, USA). Relative metabolic activities of all cell laden samples were normalized with those of hydrogels cultured for a day.

RESULTS AND DISCUSSION

Characterizations of Cellulose Nanofibers
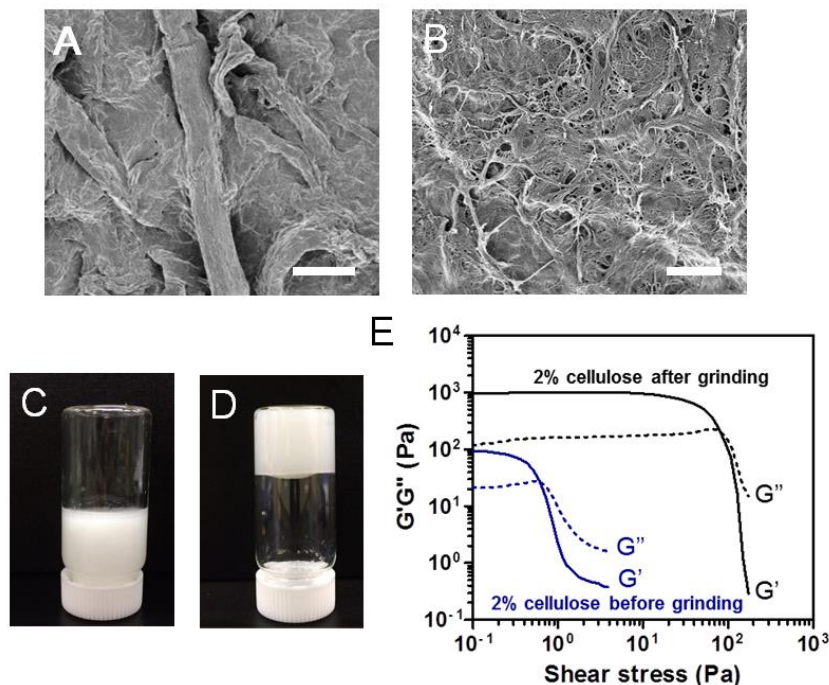
Fig. 1. SEM images before (A) (scale bar: 20 μm) and after (B) (scale bar: 2 μm) grinding pulp cellulose. Photographs of viscosity changes before (C) and after (D) grinding pulp cellulose. (E) Storage modulus and loss modulus of pulp cellulose before and after grinding

Figures 1A and 1B show the surface morphological changes of the cellulose fibers after grinding. The original pulp cellulose fibers had an average width of 20 μm (Fig. 1A), while most of the fibers turned into submicron sized fibrils after grinding for 30 passes (Fig. 1B). During the grinding process, due to different flow patterns and different force distribution to the aggregates of fibers, the fibers are heterogeneous (Ovsianikov *et al.* 2011). The differences of the morphological properties between cellulose fibers before and after the grinding process induced the differences in the rheological properties of the cellulose dispersion solutions. The 2% w/v concentration of pulp cellulose slurry before grinding had a low viscosity and showed sol-like properties (Fig. 1C). However, the same concentration of CNFs had a high viscosity and showed gel-like properties (Fig. 1D) with a high storage modulus in broad shear stress region (Fig. 1E). In contrast, pulp cellulose before grinding developed a sol state easily at low shear stress regions. The increase in the storage modulus of cellulose fibers after grinding resulted from the increase of contact area between cellulose fibers. The CNFs had large surface areas compared with the same concentration of pulp cellulose fibers, resulting in a higher possibility of hydrogen bonding and entanglement between cellulose fibers.

Rheological Properties and Printability of Bio-inks

To determine the optimal printing condition of GelMA/CNF, the fixed concentration of GelMA (5% w/v) and variable concentrations of CNF (from 0% to 2.0% w/v) were mixed, preparing five different bio-inks.
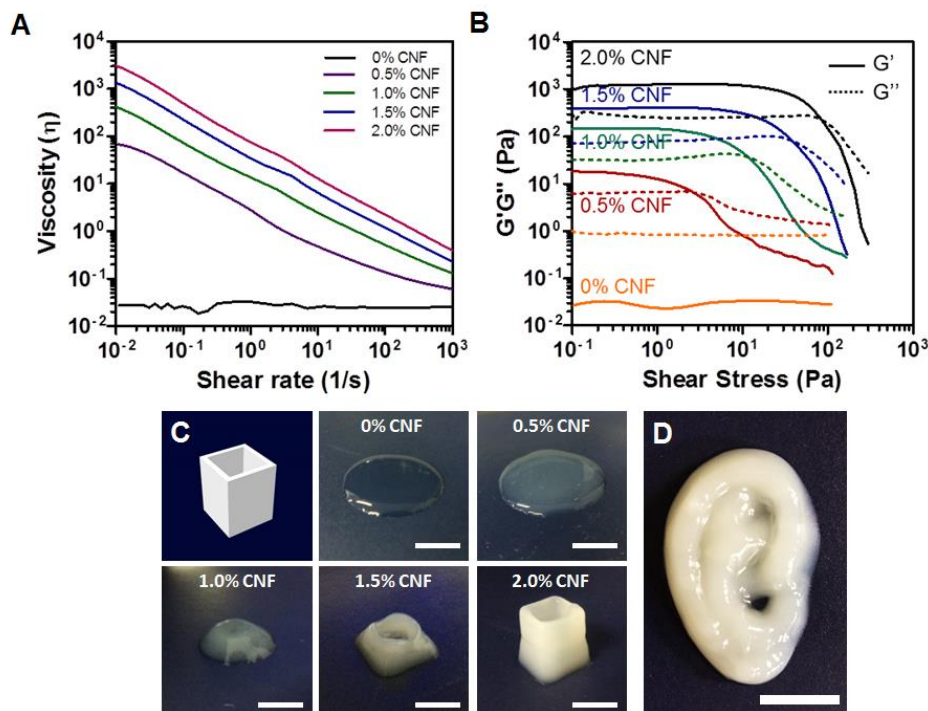
Fig. 2. Rheological properties and printability of GelMA/CNF composite inks. (A) Viscosity change at various shear rates. (B) Storage modulus changes at various shear stress. (C) Stability of hollow cube structures (scale bar: 1 cm) printed with GelMA/CNF bio-inks at the different CNF concentrations. (D) 3D printed human ear structure (scale bar: 1 cm). Different concentrations of CNF solution (0, 0.5, 1.0, 1.5, and 2.0% w/v) were prepared in cell culture medium with 5% w/v GelMA dissolved in the solutions.

The rheological properties of GelMA/CNF mixtures were characterized, and the viscosity change of the bio-inks was observed (Fig. 2A and Fig. 2B). The 5% w/v GelMA solution exhibited Newtonian behavior, with a low shear viscosity of 0.02 Pa•s. When the CNFs were incorporated with the GelMA solution, however, the printability of the GelMA solution was effectively improved. The viscosity of the GelMA solution gradually increased as the concentration of the incorporated CNFs increased. Under ambient conditions, the GelMA/CNF mixture formed a physically crosslinked gel, as reflected by the substantial increase in the shear elastic modulus (G') as the CNF concentration increased (Fig. 2B). As the concentration of CNF increased, shear stress regions at which the storage modulus (G') was larger than loss modulus ($\underline{G}$'') expanded. This ink exhibited a shear thinning behavior. This rheological response enabled the ink to be extruded through a fine nozzle, maintaining the dimensions of a filament structure during printing. Because GelMA had a low zero-shear viscosity (Fig. 2A), 5% w/v of pure GelMA bio-ink could not maintain the structure due to the poor shape fidelity in printing. As the zero-shear viscosity of the bio-ink increased by adding CNFs from 0.5% to 2.0% w/v, the shape fidelity improved. Due to the high printability and shape stability of the CNF incorporated ink, 2% w/v of CNFs incorporated into the GelMA/CNF bio-ink was appropriate to build the 3D human ear structures (Fig. 2D). During the 3D printing process, the 3D structure maintained its shape without collapsing.

Chemical Crosslinking of Printed Hydrogels
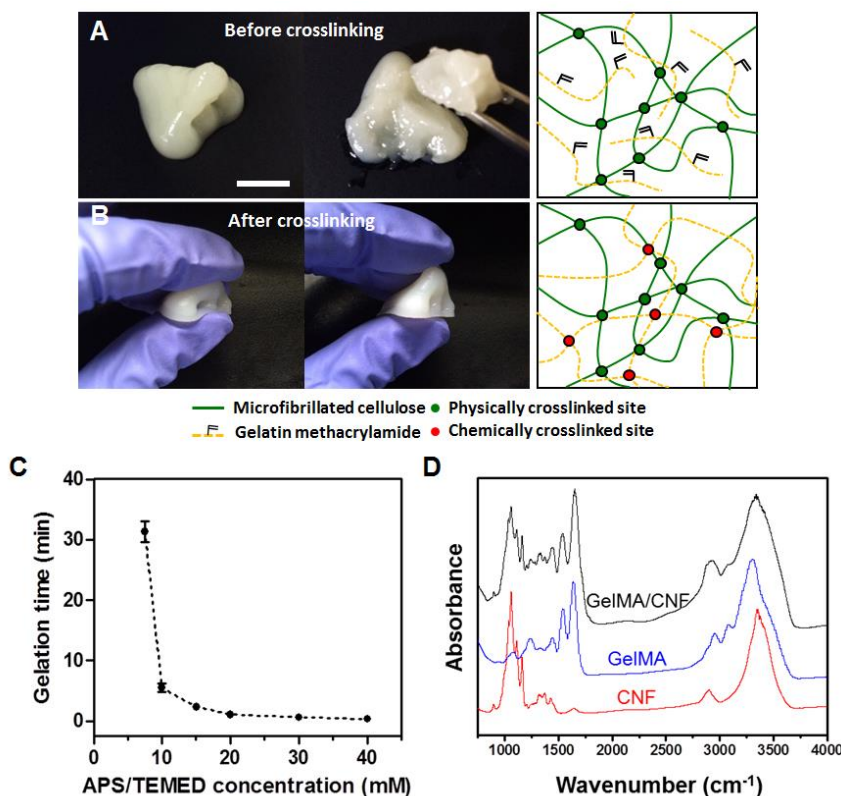
Fig. 3. Chemical crosslinking of GelMA/CNF composite bio-ink. (A) 3D printed human nose structure before chemical crosslinking of GelMA (scale bar: 1 cm). (B) Compression test of a printed nose structure after crosslinking of GelMA. (C) Variation of gelation time by APS concentrations. The same amount of TEMED as APS was added for the crosslinking. (D) FT-IR spectra for GelMA/CNF composite hydrogels

A human nose structure was successfully constructed using GelMA/CNF bio-ink (Fig. 3A). However, the printed structure was easily destroyed when outer force was applied. Immediately after printing, only the physically crosslinked sites, such as intermolecular hydrogen bonds and fiber entanglement, existed between the CNFs (Fig. 3A). Non-covalent interactions were easily broken by the applied mechanical forces, destroying the physical networks. To increase its mechanical stability, chemical crosslinking needed to be introduced to the GelMA.

Chemical crosslinking can be formed within GelMA by using a covalent bonding APS/TEMED initiating system. A chemically crosslinked GelMA/CNF composite hydrogel is shown in Fig. 3B. After GelMA/CNF was chemically crosslinked, the composite hydrogel formed interpenetrating networks (Fig. 3B) and the printed human nose structure became mechanically stable and highly elastic as a result.

The crosslinking time was influenced by the concentration of APS added to GelMA/CNF composite bio-inks (Fig. 3C). The addition of a higher amount of initiator to the printing inks decreased the crosslinking time. To apply GelMA/CNF to the bio-printing of 3D structures, it was important to control the crosslinking time to maintain the fluidity of the bio-inks during the printing step. The construction of a 20 mm × 20 mm × 20 mm hollow cube structure required approximately 20 min (0.4 mm layer height, 40% of fill density, and printing speed of 10 mm s^{-1}). When APS was added at a concentration over 15 mM, GelMA was crosslinked very rapidly. When 10 mM or 7.5 mM APS was added to the bio-ink, it took approximately 6 min and 30 min, respectively, for the crosslinking. Gelation required over 120 min when less than 5.0 mM of APS was used. As a result, the proper concentration of APS was determined depending on the printing time and the size of the structure to be printed.

The GelMA/CNF composite hydrogel was further analyzed by FT-IR (Fig. 3D). The pure GelMA hydrogel exhibited the typical amide bands of gelatin protein, including N-H stretching at 3320 cm^{-1} for amide A, C-H stretching at 3070 cm^{-1} for amide B, C=O stretching at 1657 cm^{-1} for amide I, N-H deformation at 1536 cm^{-1} for amide II, and N-H deformation at 1239 cm^{-1} for the amide III band. The CNFs exhibited a stretching vibration band of C-H at 2896 cm^{-1} to 2990 cm^{-1} and a stretching vibration band of –OH groups near 3345 cm^{-1} to 3539 cm^{-1}. The peaks of the CNFs and GelMA were observed in the composite hydrogel, confirming that the CNFs were well incorporated in the GelMA hydrogels.

Morphologies of Printed Hydrogels

The morphology of the microporous hydrogels was investigated by FE-SEM. Figure 4A shows the SEM images of freeze dried 2% w/v CNF hydrogels. The CNF hydrogels were highly porous, and the pore size ranged from 10 μm to 40 μm. The CNF aggregates formed the microscale fiber domains, which were interconnected by the entanglement between cellulose fibers (Fig. 4D). The morphology of pure GelMA hydrogel (5% w/v) also had a porous structure, denser than a CNF hydrogel (Fig. 4B). There were no fibrous structures on the surfaces of the GelMA hydrogels, and a smoother surface was observed (Fig. 4E). The hybrid hydrogels of GelMA/CNF showed a distinctive morphology from the CNFs or pure GelMA hydrogels, as illustrated in Fig. 4C. CNF macrostructures were stably bound with GelMA hydrogels. Additionally, the CNF bundles acted as a structural frame for the GelMA hydrogels, which improved the mechanical strength of the composite hydrogels. The weakness of the GelMA hydrogels could be overcome by incorporating the CNF fibrous structures.
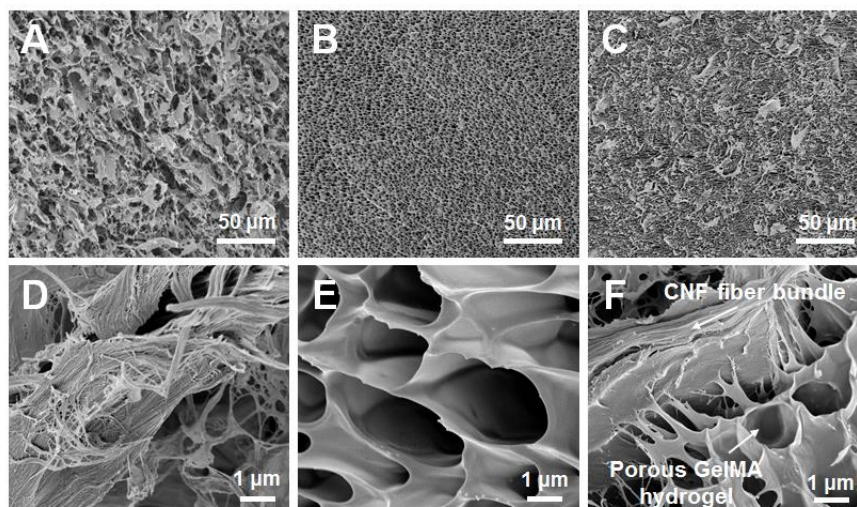
Fig. 4. Cross-sectional SEM images of 3D printed hydrogels. (A) CNF only, (B) GelMA only, (C) GelMA/CNF, (D) magnified image of (A), (E) magnified image of (B), and (F) magnified image of (C). Samples were immersed in liquid nitrogen immediately after 3D printing followed by freeze drying to maintain the porosity. APS concentration: 7.5 mM

Mechanical Properties of Hydrogels

It is critical to keep the proper mechanical strength for the biological applications of the hydrogels, especially when they are applied in the human body as implants. Hydrogels are viscoelastic materials that exhibit the properties of storing and dissipating of energy. The amount of energy stored and the amount of energy dissipated are indicated by the storage modulus (G') and the loss modulus (G''), respectively. The G' and G'' values of the GelMA/CNF composite hydrogels after chemical crosslinking are shown in Figs. 5A and 5B. The dynamic strain sweep experiments of the composite hydrogels showed a wide linear viscoelastic region. The value of the storage modulus was higher than that of the loss modulus in each case, confirming their gel state. The G' value of the GelMA/CNF composite hydrogels was higher than the pure GelMA hydrogel, indicating the increased strength of the hydrogels. The G' values of GelMA/CNF composite hydrogels gradually increased as the concentration of incorporated CNF increased because the CNFs played a reinforcing role in the composite hydrogels.

The compressive mechanical properties of the GelMA/CNF composite hydrogels were evaluated. The incorporation of CNFs in the GelMA enhanced the mechanical strength of the composite hydrogels, and the effect on the compressive modulus of hydrogels was significant as the amount of CNFs in the composite hydrogel increased (Figs. 5C and 5D). Increasing the concentration of CNF from 0.5% to 2% w/v increased the compressive modulus by almost 12-fold compared with pure GelMA hydrogels. This phenomenon resulted from the reinforcement effect induced by incorporating CNFs, which provided the structural frame of the composite hydrogels. The GelMA/CNF composite hydrogels had interpenetrating network structures.

The GelMA/CNF hydrogels containing the 3T3 fibroblast cells (CNF 2.0 C) also showed the similar viscoelastic properties to GelMA/CNF composite hydrogels (Fig. 5A and Fig. 5B). The value of the storage modulus was higher than that of the loss modulus confirming the gel state. The compressive modulus of the cell laden composite hydrogels at 2% CNF showed a lower value than the hydrogels at 2% CNF without cells. However, it showed the higher value compared with pure GelMA hydrogels (Fig. 5D).
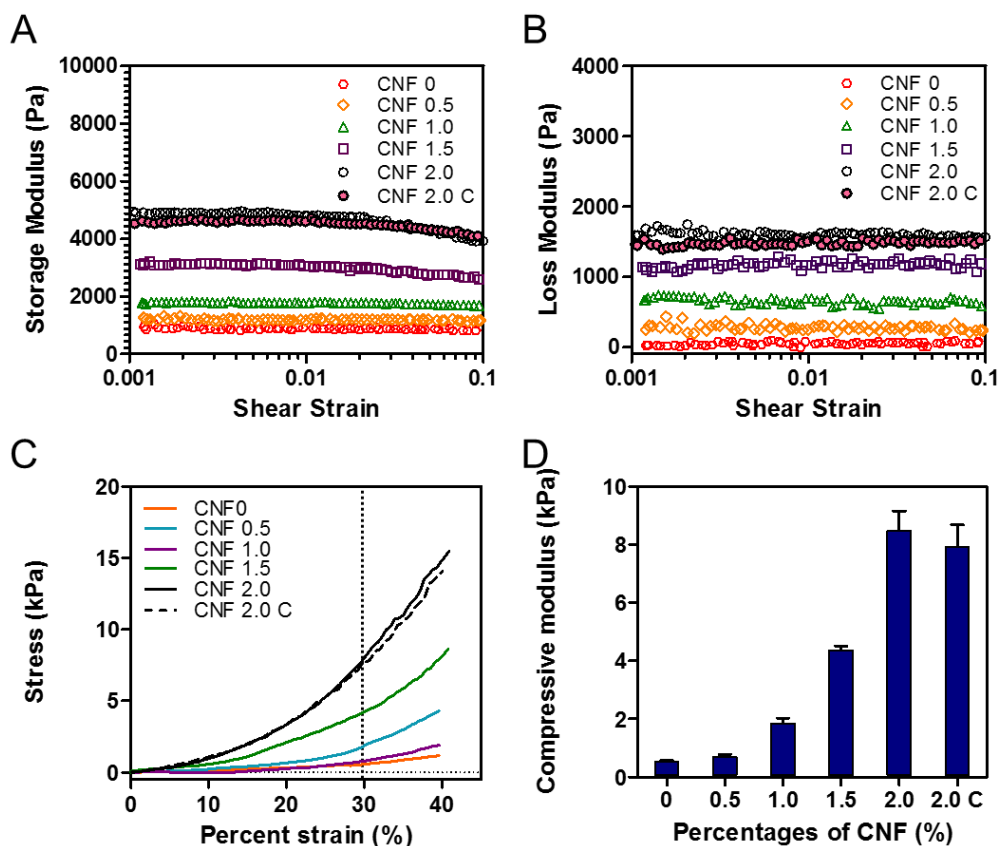
Fig. 5. Effect of CNF on the mechanical properties of GelMA/CNF composite hydrogels. (A) Storage modulus (G') and (B) loss modulus (G'') of GelMA/CNF composite hydrogels as a function of CNF concentrations. (C) Compressive stress-strain curves and (D) compressive modulus of GelMA/CNF composite hydrogels as a function of CNF concentrations. Different concentrations of CNF solution (0, 0.5, 1.0, 1.5, and 2.0% w/v) were prepared in incubation medium with 5% w/v GelMA dissolved in the solutions. 1.5×10^6 cells/mL NIH 3T3 cells were added to 5% w/v GelMA and 2% w/v CNF solution for CNF 2.0 C. APS concentration: 7.5 mM

3D Bioprinting and Cytotoxicity Analysis

A mesh structure of the hydrogel scaffolds embedded with NIH 3T3 cells was fabricated using the GelMA/CNF composite ink. The fibroblast was chosen as a model cell line to confirm the feasibility of 3D printing of GelMA/CNF bioink containing cells. It was important to fabricate 3D macroporous cells laden hydrogels because the porous structure provides a transportation path for nutrients and waste. Figure 6A shows the photographic image of the 3D GelMA/CNF hydrogel scaffolds containing NIH 3T3 cells, indicating that the 3D pore structures were maintained. As shown in Fig. 6B, the porous structure of the 3D scaffolds was observed by optical microscopy. Figures 6C through E show the live and dead cell images of the cell laden GelMA/CNF hydrogel scaffolds incubated for 1, 4, and 7 days. Green fluorescence in the cytoplasm is emitted by live cells, whereas red fluorescence is emitted in the nuclei of dead cells. The number of living cells gradually increased over the culture periods, and most cells were alive. This live and dead assay of the cell laden GelMA/CNF hydrogels indicated that the GelMA/CNF hydrogel did not have significant cytotoxicity.
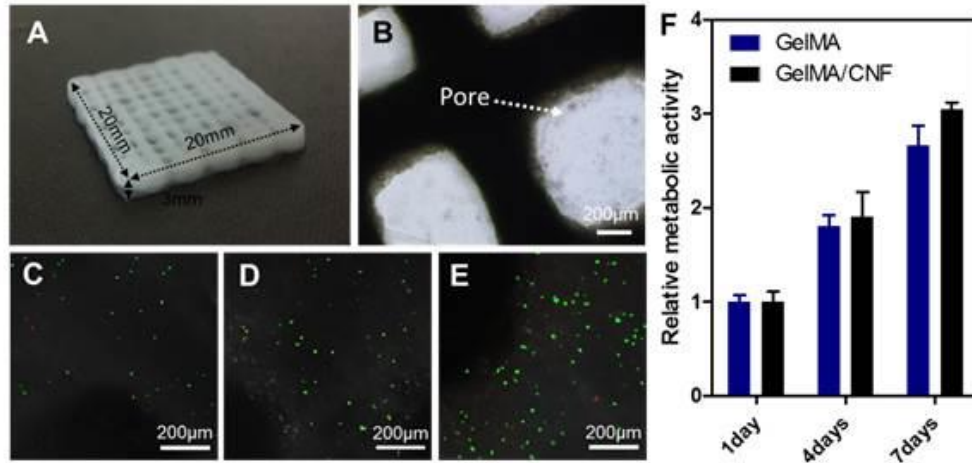
Fig. 6. Embedment of cells with 3D printed scaffolds. (A) Photograph of 3D printed meshed scaffolds embedded with NIH 3T3 cells. (B) Optical microscopic image of meshed scaffolds (scale bar: 200 μm). (C-E) Live and dead assay of embedded fibroblast cells after 1, 4, and 7 days of culturing. (F) Relative metabolic activity of NIH 3T3 cells embedded in GelMA and GelMA/CNF composite hydrogels after 1, 4 and 7 days of culturing. 1.5×10^6 cells/mL NIH 3T3 cells were added to 5% w/v GelMA and 2% w/v CNF solution for bio-ink. APS concentration: 7.5 mM

Proliferation of the encapsulated cells in the GelMA/CNF composite hydrogels was studied by an alamarBlue® assay at each time point (Fig. 6F). It was noted that cellular activity remained stable with both pure GelMA and GelMA/CNF hydrogels after the incubation for 7 days. The CNF incorporated GelMA hydrogel did not show any decrease in metabolic activity of cells. Interestingly, GelMA/CNF hydrogels showed a higher metabolic activity in comparison with pure GelMA hydrogels at longer incubation indicating the positive effect of CNFs on the cell proliferation in the hydrogel system (Fig. 6F).
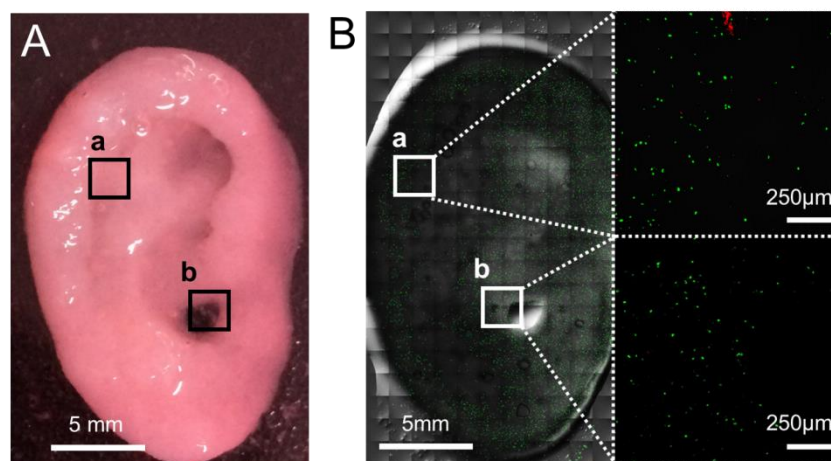
Fig. 7. Uniform distribution of cells in the 3D printed structure. (A) Photograph of cell-laden human ear structure bioprinted with GelMA/CNF after culturing for 7 days (scale bar: 5 mm). (B) Confocal laser scanning microscope images of human ear structure showing dead (red) and live (green) cells after the culture for 7 days. 1.5×10^6 cells/mL NIH 3T3 cells were added to 5% w/v GelMA and 2% w/v CNF solution for bio-ink. APS concentration: 7.5 mM

As shown in the SEM images, the CNFs allowed fibrous and porous surfaces to GelMA hydrogels. It provided cells with better attachment to the surface and the space to move through the microporous walls which were critical in cell surviving and proliferation.

A cell-laden ear structure was 3D printed, as shown in Fig. 7A. The human ear structure stably maintained its dimension for 7 days while absorbing culture medium. The cross sectional fluorescence images of the live and dead cells were observed using confocal laser scanning microscopy and the images were combined with 11×20 units (unit square 1.41 mm $\times$ 1.41 mm) (Fig. 7B). The cells were uniformly distributed through the printed ear structures, and the cells laden in the scaffolds were alive. This finding indicates that GelMA/CNF composite bio-ink was biocompatible and can be used for 3D bioprinting of biomedical scaffolds.

CONCLUSIONS

1. Due to the entanglement and hydrogen bonding between cellulose nanofibrils (CNFs), the CNF suspensions showed a high viscosity after grinding the pulp cellulose.

2. When the CNFs were incorporated into a low concentration gelatin methacrylamide (GelMA) (5% w/v) solution, the zero shear viscosity increased, and the composite bio-inks were successfully extruded in the gel state, which ensured its printability after extrusions.

3. Immediately after printing GelMA, it was crosslinked by an ammonium persulfate/ tetramethylethylenediamine (APS/TEMED) initiator system, forming covalently crosslinked stable hydrogels that could maintain their 3D structures under the applied stresses.

4. The mechanical properties of the CNFs incorporated GelMA were gradually increased when the CNF was added because the CNFs act as a structural support of the GelMA hydrogels.

5. The *in vitro* cytotoxicity test showed that the GelMA/CNF hydrogels had no cytotoxicity and high cell viability.

ACKNOWLEDGMENTS

REFERENCES CITED

Abbott, A. (2003). "Cell culture: Biology's new dimension," *Nature* 424, 870-872. DOI: 10.1038/424870a.

Abe, K., Iwamoto, S., and Yano, H. (2007). "Obtaining cellulose nanofibers with a uniform width of 15 nm from wood," *Biomacromolecules* 8, 3276-3278. DOI: 10.1021/bm700624p.

Bertassoni, L. E., Cardoso, J. C., Manoharan, V., Cristino, A. L., Bhise, N. S., Araujo, W. A., Zorlutuna, P. Vrana, N. E., Ghaemmaghami, A. M., Dokmeci, M. R., and Khademhosseini, A. (2014). "Direct-write bioprinting of cell-laden methacrylated gelatin hydrogels," *Biofabrication* 6 (2), 024105. DOI: 10.1088/1758-5082/6/2/024105.

Billiet, T., Gevaert, E., De Schryver, T., Cornelissen, M., and Dubruel, P. (2014). "The 3D printing of gelatin methacrylamide cell-laden tissue-engineered constructs with high cell viability," *Biomaterials* 35, 49-62. DOI: 10.1016/j.biomaterials.2013.09.078.

Colosi, C., Shin, S. R., Manoharan, V., Massa, S., Costantini, M., Barbetta, A., Dokmeci, M. R., Dentini, M., and Khademhosseini, A. (2016). "Microfluidic bioprinting of heterogeneous 3D tissue constructs using low-viscosity bioink," *Adv. Mater.* 28, 677-684. DOI: 10.1002/adma.201503310.

Debnath, J. and Brugge, J. S. (2005). "Modelling glandular epithelial cancers in three-dimensional cultures," *Nat. Rev. Cancer* 5, 675-688. DOI: 10.1038/nrc1695.

Dutta, R. C. and Dutta, A. K. (2009). "Cell-interactive 3D-scaffold; advances and applications," *Biotechnol. Adv.* 27, 334-339. DOI: 10.1016/j.biotechadv.2009.02.002.

Henriksson, M., Berglund, L. A., Isaksson, P., Lindstrom, T., and Nishino, T., (2008). "Cellulose nanopaper structures of high toughness," *Biomacromolecules* 9, 1579-1585. DOI: 10.1021/bm800038n.

Hollister, S. J. (2005). "Porous scaffold design for tissue engineering," *Nat. Mater.* 4, 518-524. DOI: 10.1038/nmat1683.

Loessner, D., Stok, K. S., Lutolf, M. P., Hutmacher, D. W., Clements, J. A., and Rizzi, S. C. (2010). "Bioengineered 3D platform to explore cell-ECM interactions and drug resistance of epithelial ovarian cancer cells," *Biomaterials* 31, 8494-8506. DOI: 10.1016/j.biomaterials.2010.07.064.

Markstedt, K., Mantas, A., Tournier, I., Avila, H. M., Hagg, D., and Gatenholm, P. (2015). "3D bioprinting human chondrocytes with nanocellulose-alginate bioink for cartilage tissue engineering applications," *Biomacromolecules* 16, 1489-1496. DOI: 10.1016/j.biomaterials.2010.07.064.

Mironov, V., Visconti, R. P., Kasyanov, V., Forgacs, G., Drake, C. J., and Markwald, R. R. (2009). "Organ printing: Tissue spheroids as building blocks," *Biomaterials* 30, 2164-2174. DOI: 10.1016/j.biomaterials.2008.12.084.

Murphy, S. V., and Atala, A. (2014). "3D bioprinting of tissues and organs," *Nat. Biotechnol.* 32, 773-785. DOI: 10.1038/nbt.2958.

Nichol, J. W., Koshy, S. T., Bae, H., Hwang, C. M., Yamanlar, S., and Khademhosseini, A., (2010). "Cell-laden microengineered gelatin methacrylate hydrogels," *Biomaterials* 31, 5536-5544. DOI: 10.1016/j.biomaterials.2010.03.064.

Ovsianikov, A., Deiwick, A., Van Vlierberghe, S., Dubruel, P., Moller, L., Drager, G., and Chichkov, B. (2011). "Laser fabrication of three-dimensional CAD scaffolds from photosensitive gelatin for applications in tissue engineering," *Biomacromolecules* 12, 851-858. DOI: 10.1021/bm1015305.

Park, M., Lee, D., and Hyun, J. (2015). "Nanocellulose-alginate hydrogel for cell encapsulation," *Carbohyd. Polym.* 116, 223-228. DOI: 10.1016/j.carbpol.2014.07.059.

Ruoslahti, E. (1996). "RGD and other recognition sequences for integrins," *Annu. Rev. Cell Dev. Bi.* 12, 697-715. DOI: 10.1146/annurev.cellbio.12.1.697.

Saito, T., Kimura, S., Nishiyama, Y., and Isogai, A. (2007). "Cellulose nanofibers prepared by TEMPO-mediated oxidation of native cellulose," *Biomacromolecules* 8, 2485-2491. DOI: 10.1021/bm0703970.

Sengers, B. G., Taylor, M., Please, C. P., and Oreffo, R. O. C. (2007). "Computational modelling of cell spreading and tissue regeneration in porous scaffolds," *Biomaterials* 28, 1926-1940. DOI: 10.1016/j.biomaterials.2006.12.008.

Shinoda, R., Saito, T., Okita, Y., and Isogai, A. (2012). "Relationship between length and degree of polymerization of TEMPO-oxidized cellulose nanofibrils," *Biomacromolecules* 13, 842-849. DOI: 10.1021/bm2017542.

Stelte, W., and Sanadi, A. R. (2009). "Preparation and characterization of cellulose nanofibers from two commercial hardwood and softwood pulps," *Ind. Eng. Chem. Res.* 48, 11211-11219. DOI: 10.1021/ie9011672.

Yang, J., Han, C. R., Duan, J. F., Xu, F., and Sun, R. C. (2013). "Mechanical and viscoelastic properties of cellulose nanocrystals reinforced poly(ethylene glycol) nanocomposite hydrogels," *ACS Appl. Mater. Inter.* 5, 3199-3207. DOI: 10.1021/am4001997.

Yang, J., Zhao, J. J., Xu, F., and Sun, R. G. (2013). "Revealing strong nanocomposite hydrogels reinforced by cellulose nanocrystals: Insight into morphologies and interactions," *ACS Appl. Mater. Inter.* 5, 12960-12967. DOI: 10.1021/am403669n.

Yeo, Y., Geng, W. L., Ito, T., Kohane, D. S., Burdick, J. A., and Radisic, M. (2007). "Photocrosslinkable hydrogel for myocyte cell culture and injection," *J. Biomed. Mater. Res. B.* 81B, 312-322. DOI: 10.1002/jbm.b.30667.